Endogenous γ-H2AX-ATM-Chk2 Checkpoint Activation in Bloom's Syndrome Helicase–Deficient Cells Is Related to DNA Replication Arrested Forks

V. Ashutosh Rao,[1] Chiara Conti,[1,2] Josee Guirouilh-Barbat,[1] Asako Nakamura,[1] Ze-Hong Miao,[1] Sally L. Davies,[3] Barbara Saccá,[2] Ian D. Hickson,[3] Aaron Bensimon,[2] and Yves Pommier[1]

[1]Laboratory of Molecular Pharmacology, Center for Cancer Research, National Cancer Institute, U.S. Department of Health and Human Services, Bethesda, Maryland; [2]Genome Stability Laboratory, Pasteur Institute, Paris, France; and [3]Cancer Research UK Laboratories, Weatherall Institute of Molecular Medicine, University of Oxford, John Radcliffe Hospital, Oxford, United Kingdom

Abstract

The Bloom syndrome helicase (BLM) is critical for genomic stability. A defect in BLM activity results in the cancer-predisposing Bloom syndrome (BS). Here, we report that BLM-deficient cell lines and primary fibroblasts display an endogenously activated DNA double-strand break checkpoint response with prominent levels of phosphorylated histone H2AX (γ-H2AX), Chk2 (p^{T68}Chk2), and ATM (p^{S1981}ATM) colocalizing in nuclear foci. Interestingly, the mitotic fraction of γ-H2AX foci did not seem to be higher in BLM-deficient cells, indicating that these lesions form transiently during interphase. Pulse labeling with iododeoxyuridine and immunofluorescence microscopy showed the colocalization of γ-H2AX, ATM, and Chk2 together with replication foci. Those foci costained for Rad51, indicating homologous recombination at these replication sites. We therefore analyzed replication in BS cells using a single molecule approach on combed DNA fibers. In addition to a higher frequency of replication fork barriers, BS cells displayed a reduced average fork velocity and global reduction of interorigin distances indicative of an elevated frequency of origin firing. Because BS is one of the most penetrant cancer-predisposing hereditary diseases, it is likely that the lack of BLM engages the cells in a situation similar to precancerous tissues with replication stress. To our knowledge, this is the first report of high ATM-Chk2 kinase activation and its linkage to replication defects in a BS model. (Mol Cancer Res 2007;5(7):713–24)

Introduction

Human DNA helicases have five known members that are part of the RecQ family, the loss of three of which is associated with cancer-predisposing syndromes (1). The Bloom syndrome helicase (BLM) is a member of the RecQ family of helicases that are evolutionarily conserved from *Escherichia coli* to humans. Hypomorphic mutation in the BLM protein (encoded by *RECQL3*) results in the rare, cancer-predisposing Bloom syndrome (BS, MIM number 210900; ref. 2). In addition to dwarfism, immunodeficiency, sun-sensitive telangiectatic erythma, and male infertility (3, 4), BS patients display high risk for hematologic malignancies (3, 4) as well as carcinomas (5, 6). Such predisposition to cancers is also observed in homozygous BS mice (7).

The primary defect in BLM-deficient models is suggested to be associated with the DNA replication machinery (8, 9), the main hypothesis being that BLM is involved in the restart of DNA replication-stalled forks, as recently proposed by *in vitro* studies (10). In agreement with this possibility, BLM colocalizes with the ssDNA-associated replication protein A (RPA; ref. 11) and is phosphorylated on T99 in response to replication inhibition induced by hydroxyurea and camptothecin, to which BS cells are hypersensitive (12, 13). However, only indirect data exist on the presence of stalling of replication forks in BS cells in untreated conditions, namely, the presence of repair proteins and a reduction in the replication fork rate (14-18). Additionally, the endogenous checkpoint activation that would result from these abnormal structures had not been examined until the current study.

The common cytogenetic feature of BS cells is an elevated level of sister chromatid exchanges and chromosome breaks that can be rescued by transfection with wild-type *BLM* cDNA (19-21). Because of this elevated inherent genomic instability of BS cells, BLM is considered a caretaker of the genome and essential for maintaining stability by repressing recombinational processes (18, 22-24). In agreement with this concept, elevated levels of Rad51 and Ku86 are observed in the absence of BLM, thus indicating increased homologous recombination and error-prone nonhomologous end-joining, respectively (18, 25, 26).

Received 1/17/07; revised 3/30/07; accepted 4/17/07.
Grant support: Intramural Research Program of the National Cancer Institute, Center for Cancer Research, NIH.
The costs of publication of this article were defrayed in part by the payment of page charges. This article must therefore be hereby marked *advertisement* in accordance with 18 U.S.C. Section 1734 solely to indicate this fact.
Note: Supplementary data for this article are available at Molecular Cancer Research Online (http://mcr.aacrjournals.org/).
V.A. Rao and C. Conti contributed equally to the research in this manuscript.
Competing financial interests: The authors declare that they have no competing financial interests.
Requests for reprints: Yves Pommier, 37 Convent Drive, 37-5068, NIH, Bethesda, MD 20892. Phone: 301-496-5944; Fax: 301-402-0752. E-mail: pommier@nih.gov

doi:10.1158/1541-7786.MCR-07-0028

Previous studies showed the molecular impact of BLM deficiency on DNA replication. Using bromodeoxyuridine (BrdUrd) incorporation detected under nondenaturing conditions, which reveals sites of ssDNA at aberrant replication foci, Rassool et al. (18) showed coincidence of replicating ssDNA regions with Rad51 and Ku86 foci in BS cells. BLM was also shown to colocalize with the ssDNA binding proteins, RPA (11). Such single-stranded regions can be generated by DNA replication fork stalling that results in Holliday junction intermediates. Resolution of such Holliday junctions prevents the replication forks from collapsing, which would otherwise result in illegitimate recombination (27-33). BLM also localizes in the promyelocytic leukemia nuclear bodies (34). It suppresses recombination through direct association with either Rad51 or topoisomerase IIIα (Top3α; refs. 34-37). In association with Top3α, BLM binds to and catalyzes branch migration of Holliday junctions in an ATP-dependent manner (35, 38-42). Direct interaction of BLM with Rad51 can also catalyze branch migration of the Holliday junction recombination intermediates, thus promoting double-Holliday junction dissolution by BLM-Top3α and preventing illegitimate recombinations and double-strand breaks (DSB; refs. 11, 18, 31, 34, 43).

Stalled replication forks generate DSBs and activate the intra-S checkpoint, which triggers cell cycle arrest until the damage is repaired. One of the earliest known markers of DSBs is the serine 139 phosphorylated form of the histone H2AX, called γ-H2AX (44). γ-H2AX forms macromolecular foci and marks the chromatin domain around the broken chromosomal DNA ends, thus allowing the recruitment of repair factors (45-50). Phosphoinositide-3-kinase–related kinase (PI3KK) family members ATM, ATR, and DNA-PK are responsible for the phosphorylation of H2AX (51). DNA damage promotes the phosphorylation of ATM on serine 1981 (52), which causes the dissociation of ATM dimers and the consequent activation of ATM (52, 53). Activated ATM (p^{S1981}ATM), in turn, phosphorylates the downstream kinases Chk1 and Chk2, which regulate fundamental cellular functions, such as DNA replication, cell cycle progression, and apoptosis (54-56). Chk2 is activated by ATM following its phosphorylation on T68. Chk2 then undergoes a cascade of autophosphorylation in a positive feedback loop that initiates its full activation (56-59). Growing evidence indicates functional overlap between the ATM and ATR pathways. Although ATM is considered the primary mediator of the DSB checkpoint response to ionizing radiation and radiomimetic drugs via Chk2, ATR signals after DNA replication–dependent damage by phosphorylating Chk1 (54, 55). As a consequence, one would expect activation of the ATR-Chk1 pathway in BS cells. However, previous work on the genomic instability in BS models and our own unpublished results showed no endogenous defect in basal Chk1 phosphorylation (60-62).

Constitutive phosphorylation of H2AX, ATM, and Chk2 has recently been found in human cancerous tissue samples and has also been found to be a marker of early tumorigenesis specifically in precancerous lesions (63-65). Signs of endogenous DNA damage, marked by Chk2 phosphorylation (p^{T68}Chk2) and γ-H2AX, were found in cancerous portions of the histologic sections, whereas adjoining normal tissue stained negative.

In the present study, we investigated whether the chromosomal instability caused by the absence of BLM would activate an endogenous checkpoint response. We found that BLM-deficient cells contain elevated γ-H2AX foci that colocalize with p^{S1981}ATM and p^{T68}Chk2. To address whether the endogenous checkpoint activation in unstressed BS cells is associated with DNA replication defects, we analyzed replication in BS cells using a single-molecule approach based on molecular combing and DNA analysis. Replicating DNA can be visualized following pulse-labeling with two short consecutive pulses of iododeoxyuridine (IdUrd) and chlorodeoxyuridine (CldUrd). This approach (66) allowed us to study and compare the fork length, velocity, and the interorigin distance on individual combed DNA molecules in normal and BS cells. Because the stretching factor of the combed DNA fibers is constant, we were able to convert the length of the fluorescent tracks into base pair units (67, 68). By measuring replication fork velocity and interorigin distances, we provide direct evidence for spontaneously arrested replication forks and decreased interorigin distance in BLM-deficient cells, and we show that the phosphorylated H2AX, ATM, and Chk2 colocalize with these abnormal replication sites.

Results

Endogenous Phosphorylation and Colocalization of Histone H2AX, ATM, and Chk2 in Transformed and Primary BS Cells

To examine whether the genomic instability caused by a lack of BLM activates a checkpoint response, we tested first a pair of human fibroblast cell lines, PSNG13 derived from a BS patient and its derivative, PSNF5, complemented with functional BLM (25). We also did comparative studies in untransformed BS fibroblasts (GM01492) and fibroblasts from a healthy individual (GM00037). Confocal microscopy imaging analyses were done using antibodies for phosphorylated histone H2AX (γ-H2AX), S1981 autophosphorylated ATM kinase (44, 52), and phosphorylated Chk2 at T68. We confirmed the specificity of the phosphorylated Chk2 antibody using HCT15 (Chk2 deficient) and HT29 (Chk2 proficient; ref. 69; Supplementary Fig. S1). The elevated p^{T68}Chk2 in BLM-deficient cells was also confirmed using a different antibody from Rockland Immunochemicals (Supplementary Fig. S1). All three phosphorylations γ-H2AX, p^{S1981}ATM, and p^{T68}Chk2 are known markers of DSB. Both cell types with defective BLM (PSNG13 and GM01492) showed significantly elevated levels of γ-H2AX, p^{S1981}ATM, and p^{T68}Chk2 nuclear foci (Fig. 1A) compared with their wild-type counterparts.

Quantitative analyses of the microscopy images were done to determine the distribution of the elevated nuclear signals (Fig. 1B). Foci were counted in all four cell lines from at least 30 nuclei in three independent experiments and represented as an average number per cell. Cells with functional BLM (PSNF5 and GM00037) showed significantly less cells with foci for all three phosphoproteins than the BLM-deficient cells. For example, as seen in the top graphs of Fig. 1B, ~31% of PSNG13 (BLM−) cells had between one and seven γ-H2AX foci, in contrast to 12% of PSNF5 (BLM+) cells. In PSNG13 cells, 65% of cells showed discernable foci compared with 15% in PSNF5. Similarly, 44% of GM01492 (BLM−) cells showed discernable foci compared with 20% in GM00037 (BLM+)

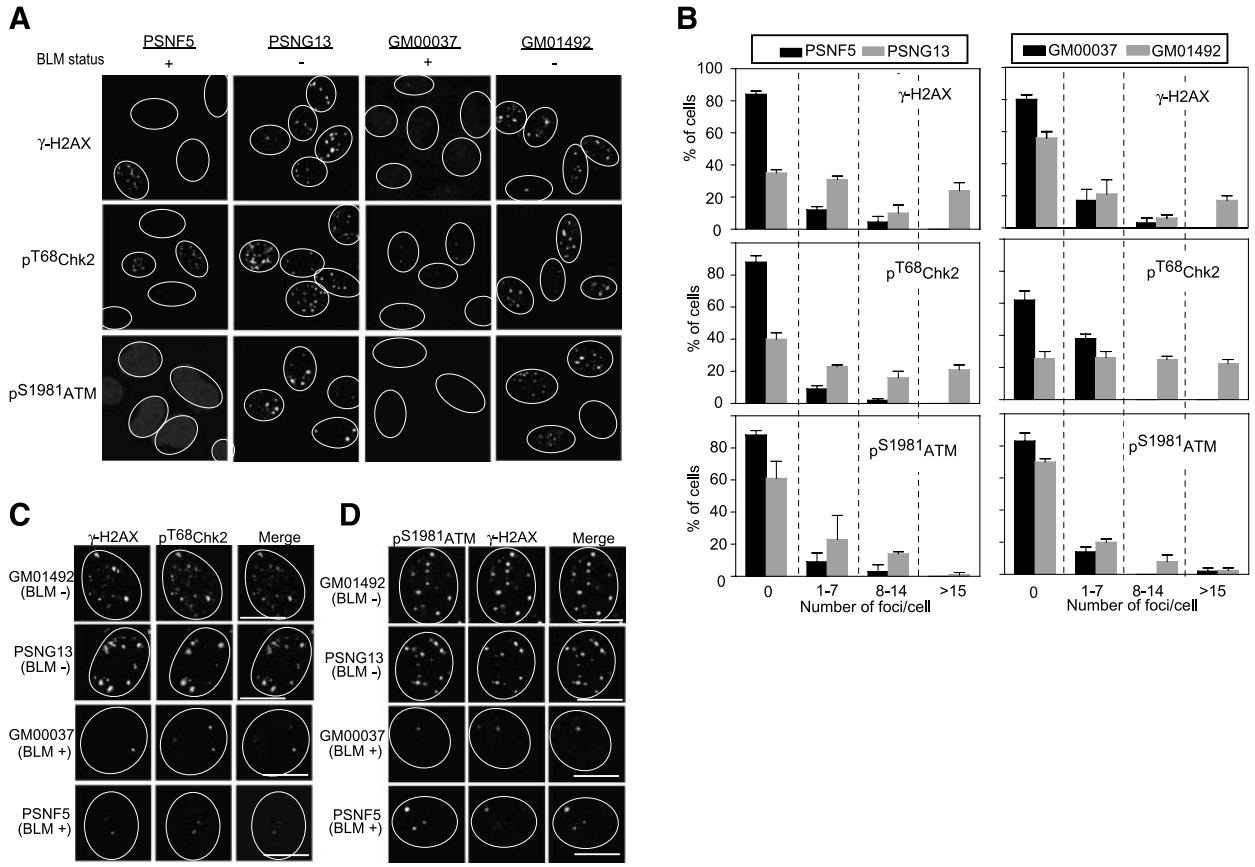

FIGURE 1. Endogenous checkpoint activation in BS cells. **A.** Transformed (*PSNG13*) and untransformed (*GM01492*) BS fibroblasts reveal endogenous γ-H2AX, p^{T68}Chk2 and p^{S1981}ATM versus their wild-type counterparts (*PSNF5* and *GM00037*, respectively). Representative confocal microscopy images of cells with wild-type (PSNF5 and GM00037) or deficient BLM (PSNG13 and GM01492) are shown. Outlines for nuclei were obtained from superimposed nuclear images of the same panel as described in Materials and Methods. **B.** Quantification of the γ-H2AX, p^{T68}Chk2 or p^{S1981}ATM foci in PSNG13 and PSNF5 cells (*left*) and GM00037 and GM01492 cells (*right*). For quantitation, a minimum of 100 cells were analyzed in at least three independent experiments. Columns, mean; bars, SD. **C.** Colocalization of γ-H2AX foci with p^{T68}Chk2 foci in BLM-deficient PSNG13 and GM01492 cells. Bottom, representative images from BLM-proficient GM00037 and PSNF5 cells were converted to black and white. **D.** Colocalization of γ-H2AX with p^{S1981}ATM foci in BLM-deficient GM01492 and PSNG13 cells. Bottom, representative images from BLM-proficient GM00037 and PSNF5. Greater than 90% colocalization was observed for γ-H2AX, p^{T68}Chk2 and p^{S1981}ATM foci. The images shown are representative examples of at least three independent experiments with at least 30 nuclei included per experimental analysis. Bar, 8 μm.

cells. Quantitation of the p^{T68}Chk2 foci in similar fashion showed elevated p^{T68}Chk2 foci in the BLM-defective PSNG13 and GM01492 cells, in contrast to PSNF5 and GM00037 cells (Fig. 1B, *middle*). Over 74% and 60% of cells stained positive for p^{T68}Chk2 foci in both PSNG13 and GM01492, respectively. In contrast, only 12% and 36% of PSNF5 and GM00037 cells stained positive for p^{T68}Chk2 foci. For p^{S1981}ATM, ~39% and 30% of PSNG13 and GM01492 cells showed elevated staining as against 12% and 17% in PSNF5 and GM00037 cells (Fig. 1B, *bottom*). Thus, BS cells exhibit high levels of nuclear foci of γ-H2AX, p^{S1981}ATM, and p^{T68}Chk2, suggesting spontaneous checkpoint activation in BLM-deficient cells, probably in response to endogenous DNA damage.

We next studied the association between γ-H2AX foci and activated ATM or Chk2 in BLM-defective (GM01492 and PSNG13) cells. Representative images are shown in Fig. 1C and D. Colocalization was observed between p^{T68}Chk2 and γ-H2AX, suggesting that the endogenously activated checkpoint protein, p^{T68}Chk2, was localized to sites of DNA damage (Fig. 1C). We also found colocalization between p^{S1981}ATM and γ-H2AX (Fig. 1D). The low levels of p^{T68}Chk2, γ-H2AX, and p^{S1981}ATM in BLM-proficient PSNF5 and GM00037 cells were also colocalized (Fig. 1C and D, *bottom*). The extent of colocalization in all panels was analyzed by measurement of the Pearson's coefficient of correlation (*r* value). The *r* value was found >0.9 between all three protein foci. No significant population with <90% colocalization was observed in three independent experiments (at least 30 nuclei per experiment). Thus, the DNA damage checkpoint in BS cells, marked by p^{S1981}ATM and p^{T68}Chk2, is found at sites of DSB as marked by γ-H2AX.

Frequency and Distribution of γ-H2AX Foci during Mitosis in BS Transformed Cells

The level of γ-H2AX has been reported to be augmented during the S phase in nonirradiated cells, thus suggesting a DNA-replication dependence for its appearance (70) and to persist during mitosis (70, 71). As we found high levels of γ-H2AX foci in BLM-deficient, in contrast to BLM-proficient cells, in interphase nuclei, we further investigated whether γ-H2AX foci were also different during mitosis as a function of

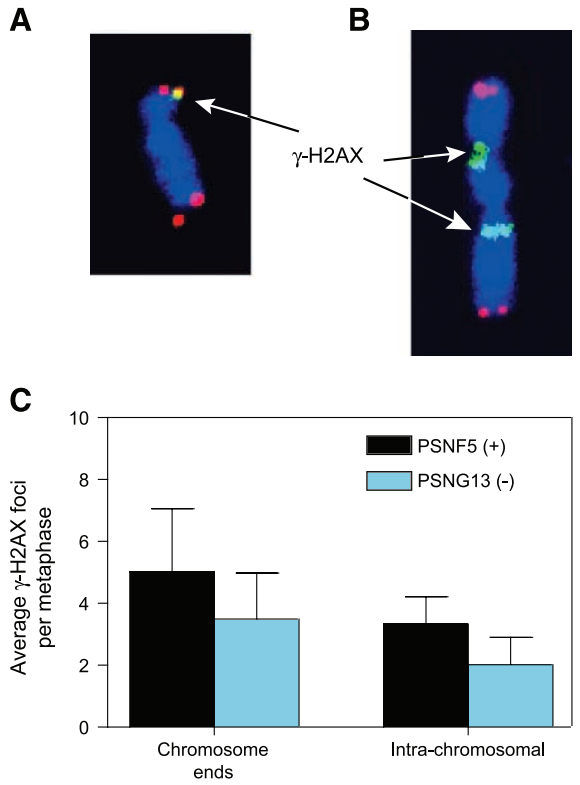

FIGURE 2. Distribution of γ-H2AX foci on metaphase spreads from BLM-proficient and BLM-deficient cells. Representative metaphase spreads were obtained from PSNF5 and PSNG13 cells. Red, telomeres labeled by fluorescence *in situ* hybridization. Green, γ-H2AX foci. Blue, chromosomes stained with DAPI. The colocalization of the red and green staining indicates a telomeric position of the γ-H2AX foci, which are referred to as chromosome-ends foci (**A**). The green signals localized within the chromosomes are referred to as intrachromosome foci (**B**). **C.** Quantification of the γ-H2AX foci per metaphase and their chromosomal distribution in BLM-proficient (*PSNF5*) and BLM-deficient (*PSNG13*) cells. The majority of the γ-H2AX foci were located at the chromosome ends in both cell lines. The percentages of chromosome-end foci were the same in both cell lines. Bars, SD of three independent experiments. Forty and thirty four metaphases were analyzed for PSNF5 and PSNG13, respectively.

BLM. The number of γ-H2AX foci was quantified on metaphase spreads obtained from transformed BLM-proficient and BLM-deficient cells (Fig. 2). We could observe γ-H2AX foci during mitosis in both the BLM-deficient PSNG13 and BLM-proficient PSNF5 cells. The telomeres were detected with a specific nucleic acid probe that recognizes telomere sequences, thus permitting us to study the distribution of the γ-H2AX foci along the chromosomes (Fig. 2A and B). The total number of foci was higher at mitosis than at interphase in both cell lines, suggesting that the population of γ-H2AX foci visible at the onset of mitosis is different from those observed in the S phase. The majority of the foci were located at the end of the chromosomes. The ratio of the telomeric versus the nontelomeric foci, referred as to "telomere end" and "intrachromosome" foci (72), respectively, was comparable in BLM-proficient and BLM-deficient cells (Fig. 2C). This result is in agreement with previous observations suggesting that BLM has a role in the telomere stability only in ALT cells, which lack the telomerase and stabilize/repair telomeres by recombination (29, 73).

Colocalization of γ-H2AX, p^{S1981}ATM, and p^{T68}Chk2 with Replication Foci

To determine whether the endogenous γ-H2AX and p^{S1981}ATM or p^{T68}Chk2 foci were localized with chromatin-replicative regions, we determined the incorporation of halogenated nucleotide (IdUrd) under nondenaturing conditions (18, 74). This assay identifies sites of replication containing ssDNA regions (ssDNA). BS cells (PNSG13 and GM01492) exhibited greater levels of IdUrd foci under these conditions, suggesting greater replicative ssDNA regions than the corresponding BLM-proficient cells (Fig. 3, *IdU*). These abnormal DNA replication sites colocalized with the γ-H2AX and p^{T68}Chk2 foci (Fig. 3A and B, *left*). There was a lack of discernable foci observed in the BLM-complemented (PSNF5) and the primary fibroblasts from a healthy individual (GM00037; Fig. 3A and B, *right*). In which case, again p^{T68}Chk2 and γ-H2AX were also present at these sites. Line scans are provided adjacent to each image to represent the extent of colocalization in the representative images. In addition, the percentage of colocalization between sites of IdUrd and γ-H2AX or pChk2 was computed and is shown in Table 1 from three independent experiments (at least 30 nuclei per experiment). We therefore propose that the endogenous DSB checkpoint activation in BS cells occurs at sites of defective replication.

Rad51, but not Top3α, Is Associated with the γ-H2AX–Associated Replication Sites in BS Cells

Previous reports showed that the absence of BLM leads to a disruption of Top3α foci formation and decolocalization of Top3α from promyelocytic leukemia bodies (13, 29). We analyzed the relationship between the IdUrd replication foci and the Top3α localization pattern in BLM-deficient cells. As expected, >95% of BS cells did not show well-defined Top3α foci (Fig. 3C). Moreover, the IdUrd foci did not colocalize well with Top3α in BS cells (Fig. 3C, *line scan*). In contrast, cells with normal BLM GM00037 showed clear Top3α foci and >90% colocalization between Top3α and the faint IdUrd foci.

We then asked whether Rad51 was associated with the abnormal replication foci present in BS cells. The Rad51 protein is involved in strand invasion and annealing of the complementary homologous strands during homologous recombination and interacts with BLM (18, 60, 75). Figure 3D shows representative images showing the accumulation of Rad51 at sites of replicative DNA damage as marked by IdUrd incorporation. The percentage of colocalization between IdUrd and Top3α or Rad51 in all cell lines studied is represented in Table 1. Collectively, these results indicate that in the presence of BLM, Top3α is concentrated at the small IdUrd sites that may correspond to minimal endogenous DNA damage, whereas in the absence of BLM, Top3α becomes diffuse from IdUrd, and under these circumstances, Rad51 and γ-H2AX are found localized to sites of replication DNA damage.

Increased Frequency of Stalled DNA Replication Forks in BS Cells

The coincidence of γ-H2AX foci with sites of replication in BLM-deficient cells, as well the elevated rate of sister

chromatid exchanges, suggested that aberrant replication could be responsible for the damages that constitutively activate ATM and Chk2 in BS cells. We therefore analyzed DNA replication in BS cells using single-DNA molecules stretched by molecular combing (66, 68). For each cell type, an asynchronous population of cells was sequentially pulse labeled, first with IdUrd, then with CldUrd, for an equal time. After combing, newly synthesized DNA, labeled with IdUrd and CldUrd, was detected with fluorescent antibodies (Fig. 4A). The use of an asynchronous population of cells avoided any artifacts introduced by the synchronization procedures, but required the collection of a large number of signals for a reliable representation of the S phase. The incorporation of two halogenated nucleotides rather than one permits unambiguous determination of the direction of the replication forks and the sites of replication firing according to the order of the fluorescent colors.

On single DNA molecules, a normal replication bubble labeled with two halogenated deoxynucleotides appears as a symmetrical fluorescent signal. In Fig. 4B, a replication bubble is formed by two forks stained in green (IdUrd pulse) and red (CldUrd pulse) and moving bidirectionally with the same velocity. A fork arrest occurring during the first pulse results in

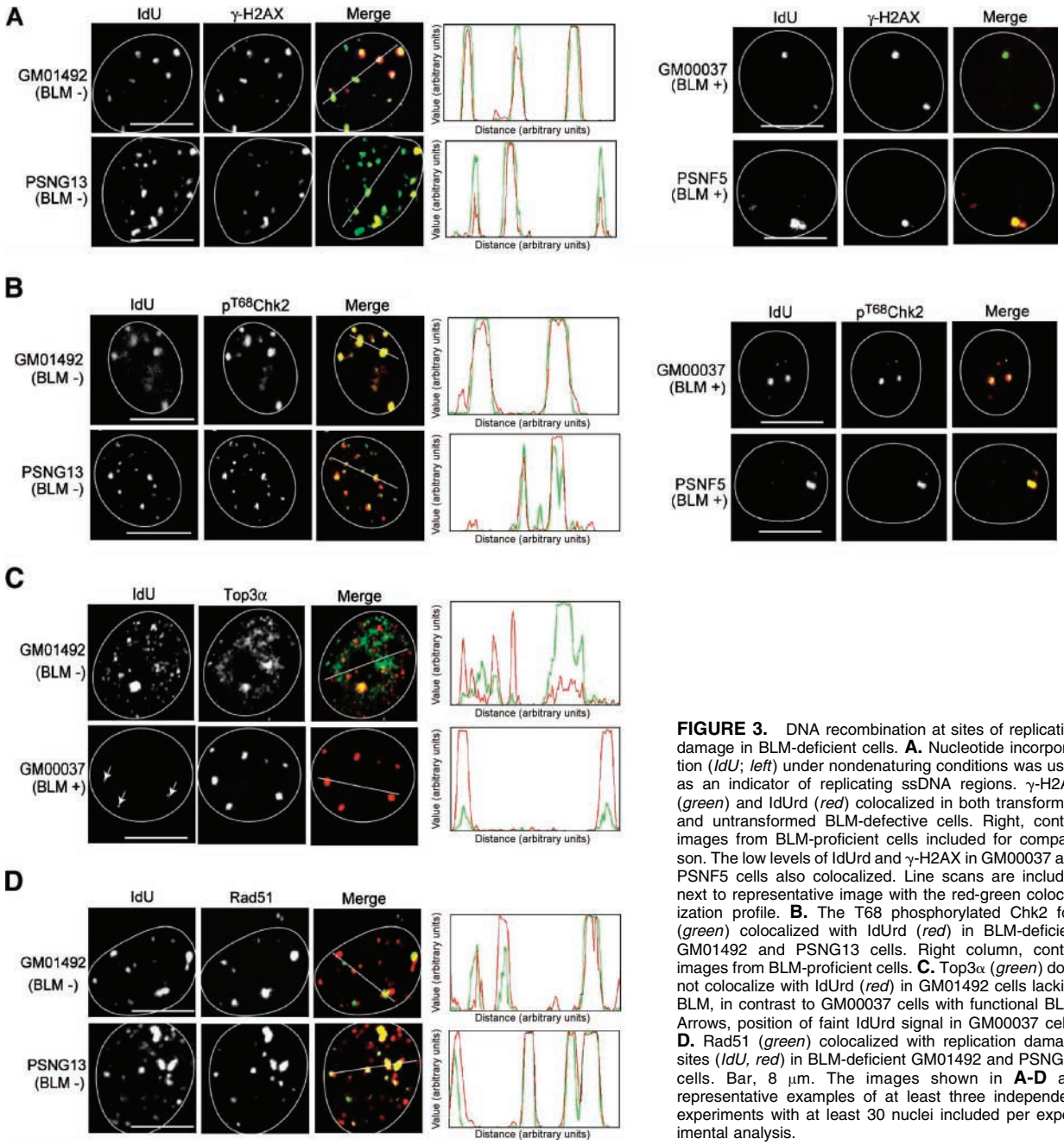

FIGURE 3. DNA recombination at sites of replication damage in BLM-deficient cells. **A.** Nucleotide incorporation (*IdU*; *left*) under nondenaturing conditions was used as an indicator of replicating ssDNA regions. γ-H2AX (*green*) and IdUrd (*red*) colocalized in both transformed and untransformed BLM-defective cells. Right, control images from BLM-proficient cells included for comparison. The low levels of IdUrd and γ-H2AX in GM00037 and PSNF5 cells also colocalized. Line scans are included next to representative image with the red-green colocalization profile. **B.** The T68 phosphorylated Chk2 foci (*green*) colocalized with IdUrd (*red*) in BLM-deficient GM01492 and PSNG13 cells. Right column, control images from BLM-proficient cells. **C.** Top3α (*green*) does not colocalize with IdUrd (*red*) in GM01492 cells lacking BLM, in contrast to GM00037 cells with functional BLM. Arrows, position of faint IdUrd signal in GM00037 cells. **D.** Rad51 (*green*) colocalized with replication damage sites (*IdU, red*) in BLM-deficient GM01492 and PSNG13 cells. Bar, 8 μm. The images shown in **A-D** are representative examples of at least three independent experiments with at least 30 nuclei included per experimental analysis.

Table 1. Percentage Colocalization of Proteins with IdUrd Foci

	BLM-deficient (%)		BLM-proficient (%)	
	GM01492	PSNG13	GM00037	PSNF5
γ-H2AX	84	87	88	92
p^{T68}Chk2	90	95	93	92
Rad51	77	68	76	82
Top3α	28	22	95	91

NOTE: Analysis included foci from at least 90 nuclei from three independent experiments.

an asymmetrical replication bubble where one fork fails to incorporate the second nucleotide (Fig. 4C, *red*). To assess the frequency of replication fork barriers in BS cells, we quantified the number of asymmetrical replication bubbles normalized to the number of total replication bubbles in BLM-proficient and BLM-deficient cells. An elevated number of asymmetries was observed in BS cells (Fig. 4D), confirming that BLM is necessary to minimize replication fork stalling.

Reduced Replication Fork Velocity in BS Cells

The molecular combing-based approach allows for the quantification of the replication fork rate by dividing the length of each fluorescent track by the incubation time with the halogenated nucleotide (Fig. 5A). Because of the constant stretching factor obtained on silanized surfaces, reproducible measurements can be obtained (68). Analyses of replication fork velocities in BLM-deficient and BLM-proficient cells showed that on any given slide obtained from one cellular sample, tracks of variable lengths were consistently noticeable. Accordingly, as shown in Fig. 5, fork velocities showed a broad distribution of values ranging from about 0.1 up to 4 kb/min. This result suggested that different regions of the genome display different fork velocities. The median of the samples does not coincide with the peak of the distribution because it is not Gaussian. Because of this broad, non-Gaussian distribution, histograms were plotted for comparison between BLM-deficient (Fig. 5B and C, *light blue*) and BLM-proficient cells (Fig. 5B and C, *dark gray*). Primary cells, irrespective of their BLM status, displayed an overall slower fork velocity when compared with the transformed cells. The median fork velocity measured in the BLM-complemented transformed PSNF5 and in the primary normal GM00037 cells was 1.34 ($n = 985$) and 1.05 kb/min ($n = 170$), respectively (Fig. 5), which is within the range measured in other human cells (76). PSNG13 displayed a median fork velocity of 1.16 kb/min ($n = 757$), and GM01492 displayed a median fork velocity of 0.76 kb/min ($n = 260$). A leftward shift for the distribution of the replication velocities was observed in BS cells, indicative of a significant reduction of replication fork velocity in both the transformed PSNG13 and the primary GM01492 BLM-deficient cell lines compared with the BLM-proficient cell lines ($P < 0.05$ by the Kolmogorov-Smirnov test and by the Mann-Whitney test).

Shorter Interorigin Distances in BS Cells

Together with the fork velocity, origin spacing is a second crucial parameter that must be regulated to ensure the complete duplication of the genome within each S phase. Interorigin distance is defined as the distance between the middle point of two replicons. The left shift of the blue columns toward smaller values observed in Fig. 6 indicates a shorter interorigin distance in BS cells, corresponding to a higher number of active origins. For each cell type, very few values could be collected for large interorigin distances. To obtain a statistical analysis, each sample was split into two subpopulations of interorigin distance for comparison (Fig. 6). The Kolmogorov-Smirnov test was used to compare values below 150 kb for the pair of transformed cells and 120 kb for the primary cells. BS cells display a significant shorter interorigin distance compared with their normal counterpart ($P < 0.05$ by the Kolmogorov-Smirnov test).

Discussion

In the past decade, the collective reporting on BS models has led to the hypothesis that BLM deficiency is primarily manifested as a DNA replication abnormality (18, 19). Endogenous genomic instability exists in untreated BS cells, which is marked by a high rate of sister chromatid exchanges (1). Our study shows that the absence of BLM also gives rise to (*a*) a constitutive γ-H2AX/ATM/Chk2 checkpoint response, (*b*) increased incidence of abnormal replicating ssDNA regions, (*c*) altered DNA replication fork velocity and interorigin distance, and (*d*) greater replication fork asymmetry suggestive of replication fork stalling.

The presence of endogenous γ-H2AX foci in untreated BS cells (Fig. 1) is indicative of abnormal levels of DSBs (44, 50, 77). The colocalization of the γ-H2AX foci with DNA replication foci, visualized by IdUrd incorporation (Fig. 3), suggests that DNA replication defects are responsible for the chromosomal breaks. Because IdUrd was detected in non-denaturing conditions, ssDNA regions are preferentially stained, thus indicating aberrant replication at those foci, as shown independently using BrdUrd incorporation (18). This endogenous activation of γ-H2AX is seemingly in contrast with our recent study showing defective induction of γ-H2AX focus formation in BS cells in response to replication-mediated DSBs induced by camptothecin treatment (13). γ-H2AX formation has also been found delayed in BS cells treated with hydroxyurea (13, 61). After exogenous replication stress, cells are likely to need BLM not only to resolve recombination intermediates when BLM functions with Top3α to resolve double-Holliday junctions (32, 38), but also to transduce a signal for greater γ-H2AX in response to DNA damage. γ-H2AX has been shown to prevent the conversion of DSBs to chromosomal breaks and translocations during class switch recombination in B lymphocytes (45, 78, 79). Furthermore, cytogenetic analyses showed that the human *H2AX* gene maps to chromosomal regions (11q23) that are altered in a relatively large number of human cancers (45). Thus, it is likely that in BS cells, under unstressed (constitutive) conditions, γ-H2AX serves to mark the sites of disrupted replication forks and to recruit other repair factors to corresponding DSBs. γ-H2AX foci have been shown to appear during the S phase and to persist in mitosis upon irradiation (70, 71). To investigate the fate of the γ-H2AX foci in untreated BLM-proficient and BLM-deficient cells, we quantified those foci and their distribution along the chromosomes of BS cells

(Fig. 2). The number of γ-H2AX foci was higher in mitosis for both the BLM-proficient and BLM-deficient cell lines, in particular in the BLM-proficient cells, which showed very little signal for γ-H2AX during interphase. Therefore, the populations of γ-H2AX foci in S and M phases are different, suggesting that the DSBs that appear during the S phase are likely repaired before entry into mitosis. Because the number of γ-H2AX foci at the onset of mitosis was comparable in the control and BS cells, BLM does not seem to be involved in the regulation and repair of mitotic DNA damage marked by γ-H2AX foci.

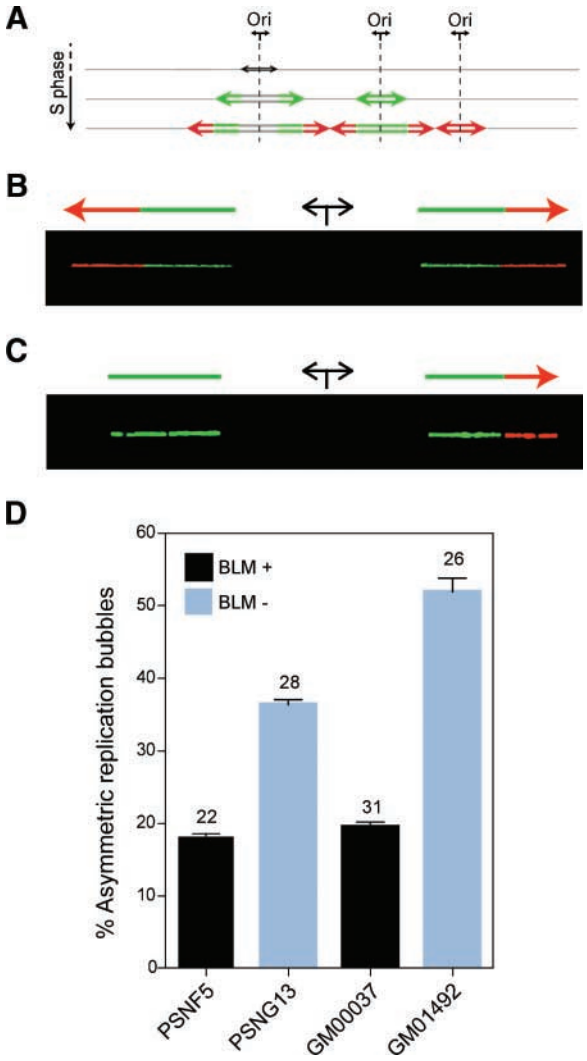

FIGURE 4. Replication fork blocks in BLM-deficient cells. **A.** Schematic representation of signals deriving from equal pulse labeling with IdUrd and CldUrd. Replication forks progress bidirectionally at the same rate from the origin and incorporate the analogues forming a symmetrical replication bubble. Upon detection of IdUrd and CldUrd, three types of signals may be obtained: (*a*) a green and red signal with a gap between the green segments, corresponding to initiations that occurred before the beginning of the pulse; (*b*) a dual-color signal with a continuous green segment corresponding to origins that fired during the first pulse; (*c*) a single isolated red signal corresponding to origins that fired during the second pulse. A continuous red signal flanked by two green ones is formed by the merging of two forks from adjacent origins. **B.** Representative image and schematic drawing of signals deriving from equal successive pulse labeling with IdUrd (*green*) and CldUrd (*red*); Replication forks progress bidirectionally at the same rate from the origin and incorporate the analogues forming a symmetrical replication signal. **C.** Representative image and schematic drawing of a replication fork arrest, detected as an asymmetrical replication signal. **D.** Histograms showing the percentages of stalled/blocked replication forks in BLM-proficient (*black*) and BLM-deficient (*blue*) cells. The number of asymmetrical replication bubbles, as shown in **C**, was divided by the total number of replication bubbles. Numbers at the top of the columns, number of events that have been counted.

Both BLM-deficient PSNG13 and GM01492 cells also displayed a clear incidence of elevated p^{S1981}ATM and p^{T68}Chk2 foci above those observed in the control PSNF5 and GM00037 cells (Fig. 1A). p^{T68}Chk2 foci were found to colocalize with γ-H2AX and IdUrd foci under nondenaturing conditions (Fig. 3), indicating that the γ-H2AX-Chk2-ATM responses occurred at replication sites with exposed single-stranded regions. In previous reports using ionizing radiation, Chk2 was phosphorylated by ATM at the sites of DNA damage (marked by γ-H2AX), but is highly mobile thereafter and does not become stably associated with the sites of DSBs (80). We observed the colocalization of p^{T68}Chk2 with IdUrd in BLM-deficient cells, which suggests that the mechanism for translocation of Chk2 might be different under exogenous and endogenous stress conditions. In precancerous as well as cancerous tissue samples, endogenous activation of Chk2 has been reported recently as a mechanism associated with replication stress in early stages of cancer, genomic instability, and selective pressure for p53 mutations (63, 64). Because BS is one of the most penetrant cancer-predisposing hereditary diseases (3), it is likely that the lack of BLM engages the cells in a situation similar to precancerous tissues with replication stress. To our knowledge, this is the first report of high ATM-Chk2 kinase activation in an untreated BS model.

Top3α, the BLM-associated topoisomerase, failed to show colocalization with replicating ssDNA sites, whereas the recombination protein Rad51 was evident at those sites in the BS cells (Fig. 3; ref. 18). This differential assembly can be explained by (*a*) the tight association between BLM and Top3α proteins in normal cells (36) and (*b*) the lack of localization of Top3α to sites of promyelocytic leukemia bodies in the absence of BLM (13, 29, 36). Therefore, in the absence of BLM, the cells probably fail to recruit Top3α to the stalled replication forks and are likely to rely on Rad51 as an alternate repair pathway. Homologous recombination would then be used to resolve aberrant DNA synthesis intermediates. The few ssDNA replication foci in BLM-proficient cells were indeed associated with Top3α (Fig. 3). Our results are in congruence with the recently proposed SOS-like hypothesis in BS cells (33). BS cells, to escape apoptotic death in the face of replication defects, trigger an alternate mode of recombination machinery (with Rad51) that involves the generation of chromosomal breaks and strand invasion and restore the assembly of functional replication forks. Such replication pauses and restarts in the absence of BLM can be expected to lower the average replication fork velocity and likely result in error-prone repair (18). The phosphorylation of H2AX and activation of the ATM-Chk2 kinase are consistent with the presence of DSBs, which may be due to frequent and/or transient replication fork pausing and repair/restart by homologous recombination.

Early studies carried out in the 1970s using DNA fiber autoradiography showed a reduced fork velocity in BS cells (14-16, 81). In the present study, we pulse labeled the cells with

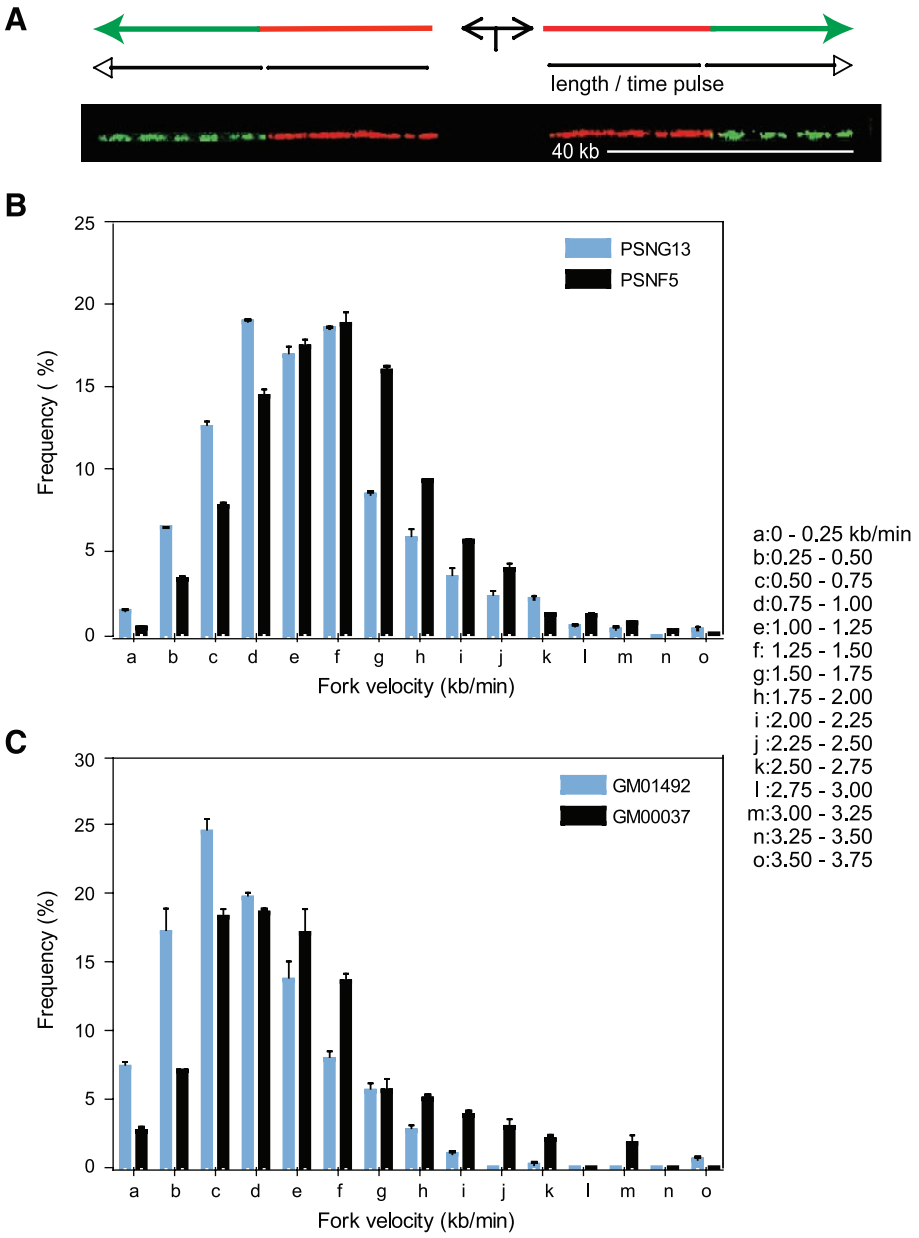

FIGURE 5. Reduced fork velocity in BLM-deficient cells. **A.** Representative image of a replicon observed on a DNA fiber after a consecutive pulse labeling with IdUrd and CldUrd, detected in red and green tracks, respectively. **A.** Scheme showing the direction of fork progression is inserted at the top. Double arrows, the origin of replication that fired at the midpoint of the gap between the red IdUrd-labeled tracks. The resulting forks progressed bidirectionally (*open arrows*), thereby generating a symmetrical replicon signal. Replication fork velocity, expressed in kilobases per minute, was obtained by measuring the length of each fluorescent track divided by the time of the pulse (40 min). White bar, 40 kb. **B.** Histogram showing replication fork velocity distribution in transformed BLM-deficient PSNG13 and in the corresponding complemented PSNF5 cells. **C.** Histogram showing fork velocity in the primary normal GM00037 and BS GM01492 primary untransformed cells. Right of **B** and **C**, ranges of fork velocity corresponding to the letters on the *X*-axis. The total number of fibers analyzed for each cell line was 985 for PSNF5, 757 for PSNG13, 170 for GM00037, and 260 for GM0001492.

two halogenated deoxynucleotides and analyzed replication fork speed and origin distribution using DNA fiber analysis by molecular combing. In agreement with the published results, our data show a reduced fork progression rate in human BLM-deficient cells. Thus, the molecular combing can be viewed as an improved and faster approach than the fiber autoradiography assays. In contrast to our current and previous findings, Versini et al. (30) showed increased fork velocity in yeast cells deficient for sgs1 (the yeast BLM homologue) when analyzing replication fork progression by molecular combing. Sgs1 is the only RecQ helicase in budding yeast, whereas human cells have five RecQs, including BLM. Additionally, Δsgs1 yeast cells display a faster progression through the S phase, contrary to human BS cells, which have a doubling time comparable to their counterpart with functional BLM. All those differences may be invoked to account for the difference in fork velocity between yeast Δsgs1 and human BLM-deficient cells. We found that, in human cells, the absence of BLM has a smaller effect in transformed cells, where a decrease of 13% was observed in the fork velocity versus the 28% in the primary cells. The transformation processes might have partially rescued from the BS phenotype, at least in the cell lines compared in this report (76). The reduced fork velocity appeared as a left shift toward smaller values in the histogram where fork speeds values are plotted (Fig. 5). This effect can be due to a real reduction of the processivity of the replication machinery and/or to an increased frequency of fork stalling. Previous studies showed that, upon replication stress, BLM is relocated at the sites of aberrant DNA replication (60, 62) and colocalizes

with a number of repairs factors after DNA replication stress (62, 82, 83). Additionally, BLM can resolve Holliday junctions, a structure generated by stalling replication forks, and has been shown to promote the regression of a replication *in vitro*, a mechanism commonly suggested for the restart of stalling fork (10). However, past analysis could not assess the frequency of stalled forks in BS cells because of technical limitations. Taking advantage of the molecular combing-based approach, we show, in this study, an increased frequency of arrested forks in BS cells, which is the first direct evidence for a role of BLM in preventing replication fork stalling *in vivo*.

We also found a shorter interorigin distance in BS cells compared with the corresponding cells with functional BLM. The difference was enhanced in primary cells, which showed a mean peak interorigin spacing ~25% shorter than BLM-deficient cells. This higher frequency of origin firing observed in BS cells can be viewed as a compensation mechanism for the slower fork progression to guarantee the full duplication of the genome without increasing the length of the S phase. Statistical analysis was done on a subset of data obtained from each cell type. The cutoff was established at 150 and 120 kb for the transformed and the primary cells, respectively, after taking into consideration the general shorter interorigin distance observed in the primary cells (Fig. 6). Those values correspond to the estimated length of chromatin loops that are anchored to the nuclear matrix by the matrix attachment regions (MAR) in a rosetta-like structure. A current model predicts that origins of replication are positioned at the MARs, at the base of the loops, which therefore form a structure to organize and regulate origins of replication in clusters (84). Previous analysis done by autoradiography of DNA fibers showed a smaller nonsignificant difference between BS and normal cells (14). The nonconstant stretching factor of the DNA molecules and the use of a single labeling as well could have affected the sensitivity of those approaches and their capability to detect subtle differences. The comparison of single loci might allow for the detection of subtle differences in the origin distribution. However, in the whole genome–scale analysis done by Hand et al. (14), the effect on the bulk interorigin distance could have been insufficient to shift the population average.

In view of the experiments presented in this report, we suggest that in the absence of BLM, cells display elevated rate of endogenous replication fork stalling, which results in the constitutive activation of the ATM-Chk2 checkpoint with the formation of γ-H2AX. Because such replicative lesions and checkpoint activation slow down the average replication fork velocity, we propose that BS cells may compensate by activating more origins of replication to complete the full replication of their genome in a timely manner.

Materials and Methods

Cell Culture

Transformed BLM-deficient (PSNG13) and *BLM*-complemented (PSNF5) fibroblasts (25) were grown in α-minimal essential medium, 10% FCS, and 350 μg/mL G418. Untransformed, primary BS fibroblasts (GM01492) and fibroblasts (GM00037) from a healthy individual were obtained from the Coriell Cell Repository and maintained in DMEM supplemented with 10% FCS. Exponentially growing cells were cultured at 37°C before experimental use.

Confocal Microscopy of Nuclear Protein Localization, Antibodies Used

Fibroblasts grown in Nunc chamber slides (Nalgene) using 0.5 mL of growth medium were fixed and permeabilized as described previously using 4% paraformaldehyde and ice-cold 70% ethanol (13). Nonspecific binding was blocked using 8% bovine serum albumin in PBS. Fixed cells were stained overnight with primary antibodies (in 1% bovine serum albumin at 4°C) and tagged with fluorescent secondary antibodies (Molecular Probes) for 2 h at room temperature. Primary antibodies for γ-H2AX were obtained from Upstate (anti-mouse) or gifted from

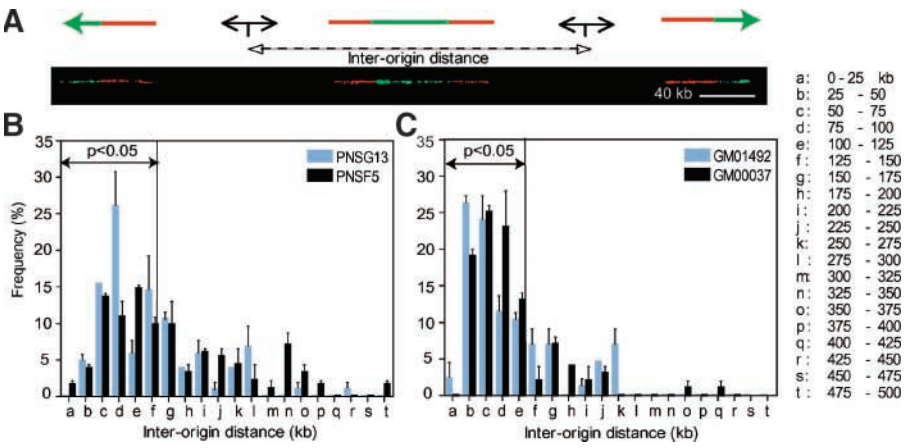

FIGURE 6. Reduced interorigin distance in BLM-deficient cells. **A.** Representative image and scheme of two adjacent replicons observed on individual DNA fibers. IdUrd was detected in red, and CldUrd was detected in green. The distance between the two origins (*short double arrows*) corresponds to the interorigin distance (*long dashed double arrows*). The central green CldUrd-labeled track results from the merge of the forks coming from the neighboring origins. White bar, 40 kb. **B.** Histogram showing interorigin distances in the transformed BLM-deficient (*PSNG13*) and in the complemented (*PSNF5*) cell lines. **C.** Histogram of the interorigin distances in the primary normal (*GM00037*) and primary untransformed BS cells (*GM01492*). Line, boundary for the statistical analysis. The Kolmogorov-Smirnov test was applied on the range of values indicated by the double-arrowed line in **B** and **C**. The total number of fibers analyzed was 92 for PSNF5, 52 for PSNG13, 50 for GM00037, and 44 for GM01492.

Dr. William Bonner (anti-rabbit). Antibodies for p^{S1981}ATM and p^{T68}Chk2 were obtained from Cell Signaling Technologies. Slides were mounted using Vectashield mounting liquid (Vector Labs) and sealed. Immunofluorescence microscopy was done in a Nikon Eclipse TE-300 confocal laser scanning microscope system. Images were collected as .tif file and processed with Adobe Photoshop (Adobe Systems Inc.). Nuclear boundaries are outlined for clarity, acquired from simultaneous images obtained after propidium iodide, 4′,6-diamidino-2-phenylindole (DAPI), or phase contrast images of the same panel. Before analysis, we did control experiments confirming the specificity of the p^{S1981}ATM and p^{T68}Chk2 antibodies in AT-deficient (GM05849) and in Chk2-deficient (HCT15) cells. The antibodies tested negative for the induction of nuclear foci in response to camptothecin or IR in these cells. The p^{T68}Chk2 antibody, from Cell Signaling Technologies, was derived using the same immunogen as the p^{T68}Chk2-specific antibody used by Lukas et al. (ref. 80; Supplementary Fig. S1).

Detection of DNA Replication Foci Using IdUrd Labeling

For the detection of ssDNA regions of replication, the incorporation of IdUrd was measured under nondenaturing conditions (18, 74, 86). Cells were preincubated for 15 min with 100 μmol/L IdUrd, followed by fixation with 4% paraformaldehyde for 20 min at room temperature and permeabilization with cold 70% ethanol at 4°C for at least 30 min. Nonspecific binding was blocked using 8% bovine serum albumin in PBS for 1 h at room temperature. After washings with PBS, cells were incubated with protein-targeted or anti-IdUrd primary antibodies from BD Biosciences (in 1% bovine serum albumin) overnight at 4°C, followed by incubation with tagged secondary antibodies (Molecular Probes Inc.) for 2 h at room temperature. The degree of colocalization was represented by the Pearson's coefficient of correlation obtained using the Simple PCI image analysis software (Compix, Inc.). Line scans for depiction of colocalization were done using Image J software (NIH).

Metaphase Spreads Preparation and Immunofluorescence Detection of Telomeres and γ-H2AX Foci

Cells were treated with demecolcine solution (Sigma, D-1925): transformed cells, 50 ng/mL of for 1.5 h at 37°C; primary cells, 100 ng/mL for 4 h (72). The medium was aspirated, and cells were gently rinsed with a hypotonic buffer [10 mmol/L Tris-HCl (pH, 7.4), 40 mmol/L glycerol, 20 mmol/L NaCl, 1 mmol/L $CaCl_2$, 0.5 mmol/L $MgCl_2$]. The hypotonic buffer was added to the cells for 15 min at 37°C. The amount of buffer depends on the concentration of cells: the optimal concentration for cytospinning is 5×10^4 cells/mL. About 200 μL of solution are added to the cytospin funnel clamped to a regular glass slide. Samples are cytospinned at 1800 rpm for 8 min. Slides are then fixed with prechilled 80% ethanol, rinsed in acetone, dried, and stored at 4°C. A hydrophobic ring is drawn around the sample area with a PapPen. Slides are rinsed in PBS 1×. Approximately 200 μL of blocking solution (8% bovine serum albumin in Ca^{2+}/Mg^{2+}-free PBS 1×) are added inside the ring, and slides are incubated 1 h at room temperature (RT) in a humid chamber. Slides are washed twice 5 min in Ca^{2+}/Mg^{2+}-free PBS 1×. About 100 μL (0.5 μL of mouse anti γ-H2AX [Upstate, 05-636] in 100 μL 10% BSA) of the first antibody inside the ring was incubated for 2 h at RT and was washed twice in Ca^{2+}/Mg^{2+}-free PBS 1×, whereas 100 μL of the second antibody (0.5 μL of anti-mouse Alex 488 [Molecular Probes] in 100 μL 10% BSA) inside the ring was incubate for 1 h at RT. These were washed thrice for 5 min in Ca^{2+}/Mg^{2+}-free TBS 1×. Exactly 100 μL of 50 mmol/L ethylene glycol-bis (E-3257, Sigma-Aldrich) were added 1 min and 10 s at RT. The slides were washed twice in Ca^{2+}/Mg^{2+}-free TBS 1×. From a telomere PNA FISH Kit/Cy3 (DAKO), 200 μL of pretreatment solution was added and incubated for 10 min. The solution was washed twice in Ca^{2+}/Mg^{2+}-free TBS 1×, and the slides were dehydrated in prechilled 70%-90%-100% ethanol. Slides are air-dried. The telomere probe solution (7.5 μL) from the DAKO kit are added inside the ring, incubated 3 min at 85°C, and incubated 1 h at RT in a humid chamber. Slides are immersed in 1× Rinse solution from the DAKO kit and incubated for 5 min at 65°C with the Wash solution. Slides are then dehydrated in prechilled 70%-90%-100% ethanol and air-dried. Slides are mounted with Vectashield containing DAPI (Vector Labs, H-1200).

DNA Molecular Combing and Statistical Analysis

In all cases, two independent sequential labelings, with IdUrd and CldUrd, were done. A subconfluent asynchronous population of cells was first labeled for 40 min with 100 μmol/L IdUrd, washed with PBS 1×, and then labeled for another 40 min with 100 μmol/L CldUrd. PBS solution and deoxynucleotide triphosphate–containing media were heated at 37°C before labeling. Cells were trypsinized, pooled, and resuspended in PBS 1× at 1% low-melting-point agarose to a final cell concentration of 1×10^5 cells/100 μL. Cells were embedded in pulsed-field gel electrophoresis agarose plugs that were kept at +4°C for 30 min to prepare a protein-free solution of high-molecular-weight genomic DNA. Agarose plugs were resuspended in a suitable volume of EDTA (250 μL per plug) and treated overnight at 50°C with 1% *N*-lauryl sarcosyl and 1 mg/mL proteinase K. Complete removal of digested proteins and other degradation products was done by several gentle washings in Tris-EDTA. Protein-free DNA plugs were then stored in EDTA at 4°C or immediately used for combing. An agarose plug was melted at 70°C for 20 min with 1.8 mL of 100 mmol/L MES (pH 6.5). The solution was kept at 42°C for 15 min and treated overnight with 2 μL β-agarase (Biolabs). The solution was dropped into a Teflon reservoir. Silanized coverslips were incubated into the DNA solution for 5 min to let DNA molecules to anchor to the coverslip, and DNA was combed using a combing apparatus (86, 87). Coverslips with combed DNA were incubated 1.5 h at 60°C and incubated in 0.5 mol/L NaOH for 10 min with gentle shaking to denature the DNA. After several quick washes in PBS 1×, coverslips were incubated with the primary antibodies. All antibodies were diluted in a 1% blocking solution (Boehringer) made in PBS 1×, incubated in a humid chamber and washed 3 × 3 min with PBS 1×. First, 2/5 mouse anti-BrdUrd (BD PharMingen) + 2/5 rat anti-CldUrd (SeraLab) were incubated for 1 h at RT. Second, 1/25 donkey anti-mouse FITC (Jackson) + 1/25 donkey anti–rat-594 (Molecular Probes) were incubated for 20 min at 37°C and mounted in Vectashield. The slides were scanned with an inverted microscope using a 60× objective. Images were

recorded by IPLab, and fluorescent signals were measured using either the home-made software Jmeasure (from the Genome Stability Laboratory at the Pasteur Institute in Paris) or ImageJ (from the National Cancer Institute). Removal of the background was done in order to allow the reader to distinguish more clearly the fluorescent signals.

Calibration of the software (ImageJ) for the measurements of the fluorescent signals. λ-DNA counterstained with YOYO-1, a fluorescent intercalating molecule that emits green fluorescence, was combed. Images of ~100 molecules were captured with a fluorescence microscope, and signals were measured in micromoles per liter with ImageJ after calibrating the software according to the camera and to the objective used. According to the known length of the λ genome,? measurements showed that 1 μmol/L = 2 kb, in agreement with previous studies (68, 87). Therefore, when combing the human genome and measuring replication fluorescent signals, an internal control to each experiment is not necessary: we calibrate the software according to the objective and the camera used, and we obtained the length in micromoles per liter that is than converted in kilobases.

Data were inserted in an Excel spreadsheet and analyzed by KyPlot and SigmaPlot. The values of fork velocity and interorigin distance were calculated for each single molecule and plotted as a frequency distribution. Statistical values of mean and median were obtained from a large set of sample data and are therefore representative of the corresponding cell population. The median corresponds to the most frequently occurring measure and is usually more informative than the mean in particular for highly skewed distributions, being less sensitive to extreme scores. Fork velocities between the samples were compared using the Kolmogorov-Smirnov test, with a significance level of $\alpha = 0.05$.

Acknowledgments

We thank Drs. Mirit Aladjem, William Bonner, Munira Amor-Gueret, Jennifer Seiler, Gabriel Eichler, and Miria Ricchetti for helpful discussions and technical assistance.

References

1. Hickson ID. RecQ helicases: caretakers of the genome. Nat Rev Cancer 2003;3:169–78.

2. German J. Bloom syndrome: a mendelian prototype of somatic mutational disease. Medicine (Baltimore) 1993;72:393–406.

3. German J. Bloom's syndrome. XX. The first 100 cancers. Cancer Genet Cytogenet 1997;93:100–6.

4. German J, Archibald R, Bloom D. Chromosomal breakage in a rare and probably genetically determined syndrome of man. Science 1965;148:506–7.

5. Gruber SB, Ellis NA, Scott KK, et al. BLM heterozygosity and the risk of colorectal cancer. Science 2002;297:2013.

6. Lowy AM, Kordich JJ, Gismondi V, Varesco L, Blough RI, Groden J. Numerous colonic adenomas in an individual with Bloom's syndrome. Gastroenterology 2001;121:435–9.

7. Luo G, Santoro IM, McDaniel LD, et al. Cancer predisposition caused by elevated mitotic recombination in Bloom mice. Nat Genet 2000;26:424–9.

8. Petkovic M, Dietschy T, Freire R, Jiao R, Stagljar I. The human Rothmund-Thomson syndrome gene product, RECQL4, localizes to distinct nuclear foci that coincide with proteins involved in the maintenance of genome stability. J Cell Sci 2005;118:4261–9.

9. Stewart E, Chapman CR, Al-Khodairy F, Carr AM, Enoch T. rqh1+, a fission yeast gene related to the Bloom's and Werner's syndrome genes, is required for reversible S phase arrest. EMBO J 1997;16:2682–92.

10. Ralf C, Hickson ID, Wu L. The Bloom's syndrome helicase can promote the regression of a model replication fork. J Biol Chem 2006;281:22839–46.

11. Brosh RM, Jr., Li JL, Kenny MK, et al. Replication protein A physically interacts with the Bloom's syndrome protein and stimulates its helicase activity. J Biol Chem 2000;275:23500–8.

12. Imamura O, Fujita K, Itoh C, Takeda S, Furuichi Y, Matsumoto T. Werner and Bloom helicases are involved in DNA repair in a complementary fashion. Oncogene 2002;21:954–63.

13. Rao VA, Fan AM, Meng L, et al. Phosphorylation of BLM, dissociation from topoisomerase IIIα, and colocalization with γ-H2AX after topoisomerase I–induced replication damage. Mol Cell Biol 2005;25:8925–37.

14. Hand R, German J. A retarded rate of DNA chain growth in Bloom's syndrome. Proc Natl Acad Sci U S A 1975;72:758–62.

15. Ockey CH. Quantitative replicon analysis of DNA synthesis in cancer-prone conditions and the defects in Bloom's syndrome. J Cell Sci 1979;40:125–44.

16. Kapp LN, Painter RB. DNA fork displacement rates in human cells. Biochim Biophys Acta 1981;656:36–9.

17. Ockey CH, Saffhill R. Delayed DNA maturation, a possible cause of the elevated sister-chromatid exchange in Bloom's syndrome. Carcinogenesis 1986;7:53–7.

18. Rassool FV, North PS, Mufti GJ, Hickson ID. Constitutive DNA damage is linked to DNA replication abnormalities in Bloom's syndrome cells. Oncogene 2003;22:8749–57.

19. Ellis NA, Proytcheva M, Sanz MM, Ye TZ, German J. Transfection of BLM into cultured bloom syndrome cells reduces the sister-chromatid exchange rate toward normal. Am J Hum Genet 1999;65:1368–74.

20. Schroeder TM. Sister chromatid exchanges and chromatid interchanges in Bloom's syndrome. Humangenetik 1975;30:317–23.

21. Chaganti RS, Schonberg S, German J. A manyfold increase in sister chromatid exchanges in Bloom's syndrome lymphocytes. Proc Natl Acad Sci U S A 1974;71:4508–12.

22. Khakhar RR, Cobb JA, Bjergbaek L, Hickson ID, Gasser SM. RecQ helicases: multiple roles in genome maintenance. Trends Cell Biol 2003;13:493–501.

23. Yankiwski V, Marciniak RA, Guarente L, Neff NF. Nuclear structure in normal and Bloom syndrome cells. Proc Natl Acad Sci U S A 2000;97:5214–9.

24. Yankiwski V, Noonan JP, Neff NF. The C-terminal domain of the Bloom syndrome DNA helicase is essential for genomic stability. BMC Cell Biol 2001;2:11.

25. Gaymes TJ, North PS, Brady N, Hickson ID, Mufti GJ, Rassool FV. Increased error-prone non homologous DNA end-joining—a proposed mechanism of chromosomal instability in Bloom's syndrome. Oncogene 2002;21:2525–33.

26. Runger TM, Kraemer KH. Joining of linear plasmid DNA is reduced and error-prone in Bloom's syndrome cells. EMBO J 1989;8:1419–25.

27. Cheok CF, Wu L, Garcia PL, Janscak P, Hickson ID. The Bloom's syndrome helicase promotes the annealing of complementary single-stranded DNA. Nucleic Acids Res 2005;33:3932–41.

28. Wang W, Seki M, Narita Y, et al. Possible association of BLM in decreasing DNA double strand breaks during DNA replication. EMBO J 2000;19:3428–35.

29. Hu P, Beresten SF, van Brabant AJ, et al. Evidence for BLM and topoisomerase IIIα interaction in genomic stability. Hum Mol Genet 2001;10:1287–98.

30. Versini G, Comet I, Wu M, Hoopes L, Schwob E, Pasero P. The yeast Sgs1 helicase is differentially required for genomic and ribosomal DNA replication. EMBO J 2003;22:1939–49.

31. Wu L, Hickson ID. RecQ helicases and topoisomerases: components of a conserved complex for the regulation of genetic recombination. Cell Mol Life Sci 2001;58:894–901.

32. Raynard S, Bussen W, Sung P. A double Holliday junction dissolvasome comprising BLM, topoisomerase IIIα, and BLAP75. J Biol Chem 2006;281:13861–4.

33. Amor-Gueret M. Bloom syndrome, genomic instability and cancer: the SOS-like hypothesis. Cancer Lett 2006;236:1–12.

34. Bischof O, Kim SH, Irving J, Beresten S, Ellis NA, Campisi J. Regulation and localization of the Bloom syndrome protein in response to DNA damage. J Cell Biol 2001;153:367–80.

35. Johnson FB, Lombard DB, Neff NF, et al. Association of the Bloom syndrome protein with topoisomerase IIIα in somatic and meiotic cells. Cancer Res 2000;60:1162–7.

36. Wu L, Davies SL, North PS, et al. The Bloom's syndrome gene product interacts with topoisomerase III. J Biol Chem 2000;275:9636–44.

37. Wu L, Davies SL, Levitt NC, et al. Potential role for the BLM helicase in

recombinational repair via a conserved interaction with RAD51. J Biol Chem 2001;276:19375–81.

38. Wu L, Hickson ID. The Bloom's syndrome helicase suppresses crossing over during homologous recombination. Nature 2003;426:870–4.

39. Cheok CF, Bachrati CZ, Chan KL, Ralf C, Wu L, Hickson ID. Roles of the Bloom's syndrome helicase in the maintenance of genome stability. Biochem Soc Trans 2005;33:1456–9.

40. Lillard-Wetherell K, Machwe A, Langland GT, et al. Association and regulation of the BLM helicase by the telomere proteins TRF1 and TRF2. Hum Mol Genet 2004;13:1919–32.

41. Karow JK, Chakraverty RK, Hickson ID. The Bloom's syndrome gene product is a 3′-5′ DNA helicase. J Biol Chem 1997;272:30611–4.

42. Karow JK, Constantinou A, Li JL, West SC, Hickson ID. The Bloom's syndrome gene product promotes branch migration of Holliday junctions. Proc Natl Acad Sci U S A 2000;97:6504–8.

43. Plank JL, Wu J, Hsieh TS. Topoisomerase IIIα and Bloom's helicase can resolve a mobile double Holliday junction substrate through convergent branch migration. Proc Natl Acad Sci U S A 2006;103:11118–23.

44. Rogakou EP, Pilch DR, Orr AH, Ivanova VS, Bonner WM. DNA double-stranded breaks induce histone H2AX phosphorylation on serine 139. J Biol Chem 1998;273:5858–68.

45. Bassing CH, Alt FW. H2AX may function as an anchor to hold broken chromosomal DNA ends in close proximity. Cell Cycle 2004;3:149–53.

46. Redon C, Pilch D, Rogakou E, Sedelnikova O, Newrock K, Bonner W. Histone H2A variants H2AX and H2AZ. Curr Opin Genet Dev 2002;12:162–9.

47. Celeste A, Petersen S, Romanienko PJ, et al. Genomic instability in mice lacking histone H2AX. Science 2002;296:922–7.

48. Fernandez-Capetillo O, Lee A, Nussenzweig M, Nussenzweig A. H2AX: the histone guardian of the genome. DNA Repair (Amst) 2004;3:959–67.

49. Paull TT, Rogakou EP, Yamazaki V, Kirchgessner CU, Gellert M, Bonner WM. A critical role for histone H2AX in recruitment of repair factors to nuclear foci after DNA damage. Curr Biol 2000;10:886–95.

50. Shroff R, Arbel-Eden A, Pilch D, et al. Distribution and dynamics of chromatin modification induced by a defined DNA double-strand break. Curr Biol 2004;14:1703–11.

51. Pilch DR, Sedelnikova OA, Redon C, Celeste A, Nussenzweig A, Bonner WM. Characteristics of γ-H2AX foci at DNA double-strand breaks sites. Biochem Cell Biol 2003;81:123–9.

52. Bakkenist CJ, Kastan MB. DNA damage activates ATM through intermolecular autophosphorylation and dimer dissociation. Nature 2003;421:499–506.

53. Bartek J, Lukas J. DNA repair: damage alert. Nature 2003;421:486–8.

54. Syljuasen RG, Sorensen CS, Hansen LT, et al. Inhibition of human Chk1 causes increased initiation of DNA replication, phosphorylation of ATR targets, and DNA breakage. Mol Cell Biol 2005;25:3553–62.

55. O'Driscoll M, Jeggo PA. The role of double-strand break repair—insights from human genetics. Nat Rev Genet 2006;7:45–54.

56. Pommier Y, Weinstein JN, Aladjem MI, Kohn KW. Chk2 molecular interaction map and rationale for Chk2 inhibitors. Clin Cancer Res 2006;12:2657–61.

57. Ahn JY, Li X, Davis HL, Canman CE. Phosphorylation of threonine 68 promotes oligomerization and autophosphorylation of the Chk2 protein kinase via the forkhead-associated domain. J Biol Chem 2002;277:19389–95.

58. Schwarz JK, Lovly CM, Piwnica-Worms H. Regulation of the Chk2 protein kinase by oligomerization-mediated cis- and trans-phosphorylation. Mol Cancer Res 2003;1:598–609.

59. Xu X, Tsvetkov LM, Stern DF. Chk2 activation and phosphorylation-dependent oligomerization. Mol Cell Biol 2002;22:4419–32.

60. Davies SL, North PS, Dart A, Lakin ND, Hickson ID. Phosphorylation of the Bloom's syndrome helicase and its role in recovery from S-phase arrest. Mol Cell Biol 2004;24:1279–91.

61. Ho CC, Siu WY, Lau A, Chan WM, Arooz T, Poon RY. Stalled replication induces p53 accumulation through distinct mechanisms from DNA damage checkpoint pathways. Cancer Res 2006;66:2233–41.

62. Sengupta S, Robles AI, Linke SP, et al. Functional interaction between BLM helicase and 53BP1 in a Chk1-mediated pathway during S-phase arrest. J Cell Biol 2004;166:801–13.

63. Bartkova J, Horejsi Z, Koed K, et al. DNA damage response as a candidate anti-cancer barrier in early human tumorigenesis. Nature 2005;434:864–70.

64. Gorgoulis VG, Vassiliou LV, Karakaidos P, et al. Activation of the DNA damage checkpoint and genomic instability in human precancerous lesions. Nature 2005;434:907–13.

65. Höglund P. DNA damage and tumor surveillance: one trigger for two pathways. Sci STKE 2006;317, pe2, 1–3.

66. Lebofsky R, Bensimon A. DNA replication origin plasticity and perturbed fork progression in human inverted repeats. Mol Cell Biol 2005;25:6789–97.

67. Herrick J, Bensimon A. Single molecule analysis of DNA replication. Biochimie 1999;81:859–71.

68. Bensimon AS, A. Chiffaudel, A. Croquette, V. Heslot, F. Bensimon. Alignment and sensitive detection of DNA by a moving interface. Science 1994; 265:2096–8.

69. Takemura H, Rao VA, Sordet O, et al. Defective Mre11-dependent activation of Chk2 by ataxia telangiectasia mutated in colorectal carcinoma cells in response to replication-dependent DNA double strand breaks. J Biol Chem 2006;281: 30814–23.

70. McManus KJ, Hendzel MJ. ATM-dependent DNA damage-independent mitotic phosphorylation of H2AX in normally growing mammalian cells. Mol Biol Cell 2005;16:5013–25.

71. Ichijima Y, Sakasai R, Okita N, Asahina K, Mizutani S, Teraoka H. Phosphorylation of histone H2AX at M phase in human cells without DNA damage response. Biochem Biophys Res Commun 2005;336:807–12.

72. Nakamura A, Sedelnikova OA, Redon C, et al. Techniques for γ-H2AX detection. Methods Enzymol 2006;409:236–50.

73. Mandell JG, Goodrich KJ, Bahler J, Cech TR. Expression of a RecQ helicase homolog affects progression through crisis in fission yeast lacking telomerase. J Biol Chem 2005;280:5249–57.

74. Raderschall E, Golub EI, Haaf T. Nuclear foci of mammalian recombination proteins are located at single-stranded DNA regions formed after DNA damage. Proc Natl Acad Sci U S A 1999;96:1921–6.

75. Braybrooke JP, Li JL, Wu L, Caple F, Benson FE, Hickson ID. Functional interaction between the Bloom's syndrome helicase and the RAD51 paralog, RAD51L3 (RAD51D). J Biol Chem 2003;278:48357–66.

76. Conti C, Saccá B, Herrick J, Lalou C, Pommier Y, Bensimon A. Replication fork velocities at adjacent replication origins are co-ordinately modified during DNA replication in human cells. MBC. In press 2007.

77. Bekker-Jensen S, Lukas C, Kitagawa R, et al. Spatial organization of the mammalian genome surveillance machinery in response to DNA strand breaks. J Cell Biol 2006;173:195–206.

78. Franco S, Gostissa M, Zha S, et al. H2AX prevents DNA breaks from progressing to chromosome breaks and translocations. Mol Cell 2006;21: 201–14.

79. Xie A, Puget N, Shim I, et al. Control of sister chromatid recombination by histone H2AX. Mol Cell 2004;16:1017–25.

80. Lukas C, Falck J, Bartkova J, Bartek J, Lukas J. Distinct spatiotemporal dynamics of mammalian checkpoint regulators induced by DNA damage. Nat Cell Biol 2003;5:255–60.

81. Hand R, German J. Bloom's syndrome: DNA replication in cultured fibroblasts and lymphocytes. Hum Genet 1977;38:297–306.

82. Wang Y, Cortez D, Yazdi P, Neff N, Elledge SJ, Qin J. BASC, a super complex of BRCA1-associated proteins involved in the recognition and repair of aberrant DNA structures. Genes Dev 2000;14:927–39.

83. Pichierri P, Franchitto A, Rosselli F. BLM and the FANC proteins collaborate in a common pathway in response to stalled replication forks. EMBO J 2004;23: 3154–63.

84. Berezney R, Mortillaro MJ, Ma H, Wei X, Samarabandu J. The nuclear matrix: a structural milieu for genomic function. Int Rev Cytol 1995;162A:1–65.

85. Rubbi CP, Milner J. Analysis of nucleotide excision repair by detection of single-stranded DNA transients. Carcinogenesis 2001;22:1789–96.

86. Conti C, Caburet S, Bensimon A. Molecular combing. In: Robinson JP, Darzynkiewicz Z, Nolan J, et al., editors. Current protocols in cytometry. New Jersey: John Wiley & Sons; 2003. p.8.10.1–8.10.23.

87. Michalet X, Ekong R, Fougerousse F, et al. Dynamic molecular combing: stretching the whole human genome for high-resolution studies. Science 1997; 277:1518–23.